predict ε-Fe should not order magnetically (24), suggesting that it is paramagnetic.

The estimated values of χ offer constraints on existing models of Earth's magnetic field behavior, provided they remain valid at high core temperatures (4000° to 8000°C) and pressures (330 to 360 GPa). A paramagnetic inner core can explain a variety of geomagnetic phenomena (4), the source of which cannot be ascribed to processes acting in the outer core. The results of Hollerbach and Jones (1) and the recently developed three-dimensional dynamic models of Glatzmaier and Roberts (2) predict that a finitely conducting solid inner core would stabilize the geodynamo, because the inner core has a diffusive time scale independent of that of the outer core. We speculate the same could be true if the paramagnetic relaxation time of the inner core lags behind external field changes from the outer core. The outcome is that short-term fluctuations are damped out, and the dynamo is steadied. As a result, a brief breakdown of the dynamo would not lead to a successful reversal of the field. This inhibition to reversal, which results directly from the inner core's stabilizing influence on outer core convection, is feasible if our estimates are valid at core temperatures.

REFERENCES AND NOTES

1. K. Hollerbach and C. Jones, *Nature* **365**, 541 (1993).
2. G. Glatzmaier and P. Roberts, *ibid.* **377**, 203 (1995).
3. R. Merrill, M. McElhinny, D. Stevenson, *Phys. Earth Planet. Inter.* **20**, 75 (1979); X. Quidelleur, J. Valet, V. Courtillot, G. Hulot, *Geophys. Res. Lett.* **21**, 1639 (1994).
4. B. Clement and L. Stixrude, *Earth Planet. Sci. Lett.* **130**, 75 (1995).
5. A. Morelli, A. Dziewonski, J. Woodhouse, *Geophys. Res. Lett.* **13**, 1545 (1986); P. Shearer, K. Toy, J. Orcutt, *Nature* **333**, 228 (1988); X. Song and D. Helmberger, *Geophys. Res. Lett.* **20**, 2591 (1993).
6. O. Anderson, *Geophys. J. R. Astron. Soc.* **84**, 561 (1986); J. Brown and R. McQueen, *J. Geophys. Res.* **91**, 7485 (1986); H. Mao, P. Bell, C. Hadidiacos, in (7), pp. 135–138; Q. Williams, R. Jeanloz, J. Bass, B. Svendsen, T. J. Ahrens, *Science* **236**, 181 (1987); M. Ross, D. Young, R. Grover, *J. Geophys. Res.* **95**, 21713 (1990); C. S. Yoo, J. Akella, A. J. Campbell, H. K. Mao, R. J. Hemley, *Science* **270**, 1473 (1995).
7. S. Akimoto, T. Suzuki, T. Yagi, O. Shimomura, in *High-Pressure Research in Mineral Physics*, M. H. Manghnani and Y. Syono, Eds. (Geophysical Monograph 39, American Geophysical Union, Washington, DC, 1987), pp. 149–154.
8. M. H. Manghnani, L. Ming, N. Nakagiri, *ibid.*, pp. 155–163; R. Boehler, *Geophys. Res. Lett.* **13**, 1153 (1986).
9. H. Wenk, T. Takeshita, R. Jeanloz, G. Johnson, *Geophys. Res. Lett.* **15**, 76 (1988).
10. R. Jeanloz and H. Wenk, *ibid.*, p. 72.
11. S. Karato, *Science* **262**, 1708 (1993).
12. D. Farrell *et al.*, *Phys. Rev. B* **36**, 4025 (1987); P. DeRango *et al.*, *Nature* **349**, 770 (1991).
13. E. Collings and J. Ho, *Phys. Rev. B* **2**, 235 (1970); É. Volkenshteĭn, V. Galoshina, N. Shchegolikhina, *Sov. Phys. JETP* **29**, 79 (1969); L. Stixrude and R. E. Cohen, *Science* **267**, 1972 (1995).
14. D. Adams, R. Appleby, S. Sharma, *J. Phys. E* **9**, 1140 (1976).
15. D. Collinson, *Methods in Rock Magnetism and Paleomagnetism* (Chapman & Hall, New York, 1983).
16. E. Huang, W. Bassett, P. Tao, in (7), pp. 165–172; A. Jephcoat, H. Mao, P. Bell, *J. Geophys. Res.* **91**, 4677 (1986); W. Bassett and M. Weathers, *ibid.* **95**, 21709 (1990).
17. N. Von Bargen and R. Boehler, *High Pressure Res.* **6**, 133 (1990).
18. J. Happel and H. Brenner, *Low Reynolds Number Hydrodynamics* (Nijhoff, Boston, ed. 4, 1986).
19. K. Stephan and K. Lucas, *Viscosity of Dense Fluids* (Plenum, New York, 1979).
20. M. Rouault, *Électricité* (Masson, Paris, 1965).
21. P. Wasilewski, *Adv. Earth Planet. Sci.* **1**, 123 (1977).
22. H. Ohno, *J. Phys. Soc. Jpn.* **31**, 92 (1971); H. Ohno and M. Mekata, *ibid.*, p. 102; D. Pearson and J. Williams, *J. Phys. F* **9**, 1797 (1979).
23. R. Taylor, G. Cort, J. Willis, *J. Appl. Phys.* **53**, 8199 (1982); G. Cort, R. Taylor, J. Willis, *ibid.*, p. 2064; R. Taylor, M. Pasternak, R. Jeanloz, *ibid.* **69**, 6126 (1991).
24. G. Fletcher and R. Addis, *J. Phys. F* **4**, 1951 (1974).
25. The generosity and guidance of E. Knittle and grants from the Earth Sciences Department, University of California, Santa Cruz, made this study possible. We thank S. Bigot, R. Coe, V. Courtillot, C. Jaupart, E. Knittle, M. LeGoff, J. Peyronneau, J. P. Poirier, and two anonymous reviewers for helpful discussions and comments. Institut de Physique du Globe de Paris contribution 1502.

14 August 1997; accepted 7 November 1997

Formation of Molecular Chlorine from the Photolysis of Ozone and Aqueous Sea-Salt Particles

K. W. Oum, M. J. Lakin, D. O. DeHaan,* T. Brauers,†
B. J. Finlayson-Pitts‡

Halogen atoms from the reactions of sea-salt particles may play a significant role in the marine boundary layer. Reactions of sodium chloride, the major component of sea-salt particles, with nitrogen oxides generate chlorine atom precursors. However, recent studies suggest there is an additional source of chlorine in the marine troposphere. This study shows that molecular chlorine is generated from the photolysis of ozone in the presence of sea-salt particles above their deliquescence point; this process may also occur in the ocean surface layer. Given the global distribution of ozone, this process may provide a global source of chlorine.

Sea-salt particles formed by wave action are ubiquitous in the marine boundary layer and in coastal regions. In addition, they have been found in some unusual situations such as in the plumes from the burning of the Kuwaiti oil wells (1). Chlorine atoms (Cl) formed from the reactions of sea-salt particles can destroy ozone (O_3), a key tropospheric oxidant (2–7) and greenhouse gas (8), through direct reaction. Alternatively, Cl reacts rapidly with organic molecules, which can, in turn, lead to O_3 formation in the presence of sufficient oxides of nitrogen (NO_x) (9).

Laboratory (2, 6, 7) and modeling (5, 10, 11) studies have shown that photochemically active, gas-phase Cl- and Br-containing compounds can be generated by a number of reactions of sea salt and its components. Although HNO_3 and H_2SO_4 displace HCl from sea-salt particles, this is not a significant source of atomic Cl because the subsequent reaction of HCl with OH is relatively slow (12). Furthermore, the reactions of acids and oxides of nitrogen are insufficient under some circumstances to account for the measured Cl^- depletion (13), and a photochemical reaction of O_3 with aqueous sea-salt particles has been suggested as an alternative way of generating Cl_2. Although O_3 does not react at a significant rate with dry NaCl (14), laboratory studies have suggested that an unidentified photolyzable Cl-containing compound may form from sea-salt particles close to the deliquescence point in the presence of O_3 and probably light (15).

Field studies have identified photochemically active, gas-phase halogen compounds other than HCl in the troposphere (16–20), but specific compounds have been difficult to identify. Recently, Cl_2 was identified and measured in a coastal area (21) at concentrations up to 150 parts per trillion (ppt). This is a much larger concentration than can be attributed to known reactions of sea-salt particles, suggesting that there must be an unrecognized source producing a daily average of 280 ppt of Cl_2 per day.

We report the specific identification of Cl_2 as the product of the photolysis of O_3 in the presence of aqueous sea-salt particles in a controlled laboratory experiment. We used an aerosol chamber of 561 liters vol-

---

Department of Chemistry, University of California, Irvine, CA 92697-2025 USA.

*Present address: Department of Chemistry and Biology, Lyon College, Post Office Box 2317, 2300 Highland Road, Batesville, AR 72503-2317, USA.
†Present address: Institut für Atmosphärische Chemie, Forschungszentrum KFA, 52425 Jüelich, Germany.
‡To whom correspondence should be addressed. E-mail: bjfinlay@uci.edu

ume in our experiments (*22*). We monitored the reactants and products during the run, using infrared and ultraviolet (UV)-visible spectrometry (*23*) as well as atmospheric-pressure ionization mass spectrometry (API-MS) (*24*). We generated polydisperse sea-salt aerosols using a commercial system (TSI, Inc.) consisting of an atomizer (model 3076), a differential mobility analyzer (DMA) (model 3071), and an ultrafine condensation particle counter (model 3025). A 1.0% (w/w) solution of synthetic sea salt (Instant Ocean, Aquarium Systems, Mentor, Ohio) was atomized and dried with a diffusion dryer, and we measured the size distribution using the DMA. The DMA was then bypassed, and the dried polydisperse aerosol particles were added to the chamber containing air at a relative humidity (RH) in the range of 86 to 90% at 298 K, which caused the particles to deliquesce. A typical particle number concentration in humidified air in the chamber was 5×10^4 particles per cubic centimeter with a geometric number mean diameter of 150 nm and a geometric standard deviation σ of 1.9. Then O_3 was added to the chamber to give initial concentrations before photolysis of 0.8 to 14 parts per million (ppm). After the reaction was followed in the dark, the bank of UV lights was turned on to photolyze the mixture for measured time periods. Before and after each photolysis period, the chamber contents were analyzed by API-MS and Fourier transform infrared spectroscopy (FTIR).

We observed Cl_2 only when O_3, sea-salt particles above their deliquescence point, and light were present (Fig. 1); Cl_2 was not generated in blank runs with O_3, aerosol particles, or both in the dark or with irradiated sea-salt particles alone. As seen in Fig. 1, Cl_2 was produced rapidly when the mixture of wet sea-salt particles and O_3 was photolyzed. We also observed the formation of small amounts of Cl_2 when we used dry sea-salt particles. However, these particles are known to have large amounts of surface-adsorbed water (*25*), and hence the same chemistry is likely occurring in the film of surface water.

We confirmed that the peaks at a mass-to-charge ratio (*m*/*e*) of 70, 72, and 74 were a result of Cl_2, using MS-MS scans (Fig. 2). As expected, collisional dissociation of the ion at *m*/*e* = 70 gave a fragment at 35 atomic mass units (amu) (Fig. 2A), *m*/*e* = 72 gave fragments at 35 and 37 amu (Fig. 2B), and *m*/*e* = 74 gave a fragment at 37 amu (Fig. 2C). A further check was carried out in which the sample was passed through an annular denuder coated with K_2CO_3 to remove Cl_2; the peaks attributed to Cl_2 disappeared. We also carried out experiments using NaCl particles, and we observed Cl_2 generation at similar rates.

To ensure that Cl_2 formation was not due to an unrecognized chamber artifact, we also carried out some studies with sea-salt particles and a clean 70-liter Teflon reaction chamber. We observed Cl_2 formation under the same conditions as in the larger aerosol chamber.

The formation of Cl_2 was limited by the availability of O_3. Thus, the rate of formation of Cl_2 declined as the O_3 was destroyed by photolysis and ceased when the O_3 was gone. Generation of Cl_2 resumed when more O_3 was added. At an initial O_3 concentration of 14 ppm, approximately 45 parts per billion (ppb) Cl_2 were formed in the first 2 min of photolysis, and Cl_2 concentrations peaked at ~100 ppb when the O_3 was depleted. Experiments were carried out at O_3 concentrations down to ~0.8 ppm. Smaller peak concentrations of Cl_2 (~10 ppb) were produced as O_3 was rapidly depleted.

In summary, O_3, light, and aqueous particles containing Cl^-, either from sea salt or from NaCl, are necessary for the formation of Cl_2. One potential reaction mechanism involves oxidation initiated by OH in the aqueous phase of the particles as suggested earlier by Keene *et al.* (*16*). It is known that OH is generated in the aqueous-phase photochemistry of dissolved O_3 (*26*–*30*):

$$O_{3(aq)} + h\nu(\lambda = 254\text{ nm}) \xrightarrow{H_2O} H_2O_{2(aq)} + O_2 \quad (1)$$

$$H_2O_{2(aq)} + h\nu(\lambda = 254\text{ nm}) \rightarrow 2OH_{(aq)} \quad (2)$$

where λ is the wavelength of light. Alternatively, H_2O_2 and OH can be generated in the gas phase and then be taken up into the particle aqueous phase:

$$O_{3(g)} + h\nu(\lambda = 254\text{ nm}) \rightarrow O(^1D)_{(g)} + O_{2(g)} \quad (3)$$

$$O(^1D)_{(g)} + H_2O_{(g)} \rightarrow 2OH_{(g)} \quad (4)$$

$$OH_{(g)} \rightarrow OH_{(aq)} \quad (5)$$

$$OH_{(g)} + O_{3(g)} \rightarrow HO_{2(g)} + O_{2(g)} \quad (6)$$

$$HO_{2(g)} + HO_{2(g)}\ (+M, H_2O) \rightarrow H_2O_{2(g)} + O_{2(g)} \quad (7)$$

$$H_2O_{2(g)} \rightarrow H_2O_{2(aq)} \quad (8)$$

$$H_2O_{2(aq)} + h\nu(\lambda = 254\text{ nm}) \rightarrow 2OH_{(aq)} \quad (2)$$

Then OH oxidizes Cl^- in the aqueous phase:

$$OH + Cl^- \leftrightarrow HOCl^- \quad (9a, 9b)$$

$$HOCl^- + H^+ \rightarrow Cl + H_2O \quad (10)$$

$$Cl + Cl \rightarrow Cl_2 \quad (11)$$

$$Cl + Cl^- \rightarrow Cl_2^- \quad (12)$$

$$Cl_2^- + Cl_2^- \rightarrow Cl_2 + 2Cl^- \quad (13)$$

$$Cl_2 + H_2O \rightarrow HOCl + H^+ + Cl^- \quad (14)$$

$$HOCl + H^+ + Cl^- \rightarrow Cl_2 + H_2O \quad (15)$$

The dissociation of $HOCl^-$ back to OH + Cl^- (reaction 9b) occurs in competition with its reaction with H^+ to generate Cl atoms (reaction 10), and at neutral pH the dissociation is much faster (*31*). Reactions 9a and 9b are in essence an equilibrium, and Cl atoms are generated when the rate-determining reaction 10 of $HOCl^-$ with H^+ occurs. At least a portion of the Cl_2 is released to the gas phase.

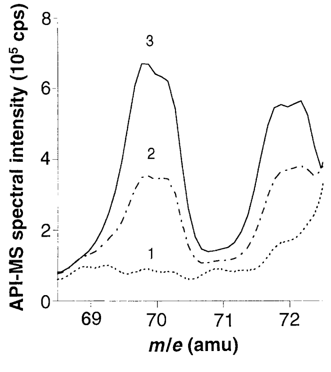

Fig. 1. Peaks at *m*/*e* = 70, 72 as measured with API-MS (Q1 scan, 25 scans coadded) in the reaction of O_3 (14 ppm) with a polydisperse sea-salt aerosol (geometric mean diameter = 150 nm, σ = 1.9) at 86% RH and 298 K in air: curve 1, from O_3 and wet sea-salt particles in the dark; curve 2, after irradiating (λ = 254 nm) for 2 min; curve 3, after 10-min photolysis. The higher background at *m*/*e* = 72 is because of a small contribution from a contaminant peak at *m*/*e* = 73 (cps, counts per second).

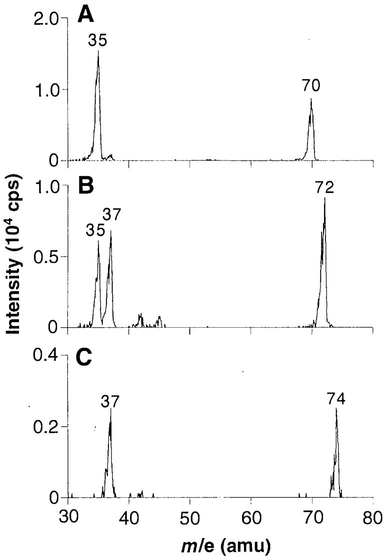

Fig. 2. MS-MS scans (40 scans coadded) of the peaks at (**A**) *m*/*e* = 70, (**B**) *m*/*e* = 72, and (**C**) *m*/*e* = 74 after irradiation for 10 min of O_3 and a polydisperse sea-salt aerosol in air at 86% RH and 298 K.

Quantitative extrapolation of these results to atmospheric conditions must be carried out with caution. The O_3 and aerosol number concentration were higher in these experiments than in the marine boundary layer, and, in addition, the light intensity and photolysis wavelength distribution differ. The highest O_3 concentration we used was 14 ppm, which generated 45 ppb of Cl_2 in 2 min. If the concentration of the oxidant for Cl^- is proportional to the O_3 concentration (*32*), 14 ppm O_3 would have generated 400 times the amount of Cl_2 expected under a typical marine boundary layer O_3 concentration of ~35 ppb.

If aqueous-phase chemistry predominates, the important aerosol parameter is the volume of liquid phase available for reaction. The typical sea-salt particle diameter of 0.15 μm used in our experiments is much smaller than that of a typical sea-salt particle (1 to 4 μm) in the marine boundary layer (*33–35*). However, the total aqueous-phase volume available for reaction is similar because of the much larger number concentration of particles in these chamber experiments, 5×10^4 particles per cubic centimeter compared to 1 to 10 particles per cubic centimeter in the marine boundary layer (*33–35*). Thus, no correction was applied for differences in available particle aqueous-phase volume.

We used radiation of 254-nm wavelength in these experiments. Although the actinic cutoff at Earth's surface is 290 nm (*9*), the use of 254 nm radiation provided efficient photolysis of O_3 at a wavelength that was not absorbed significantly by Cl_2. As a result, the buildup of Cl_2 during the reactions could be readily observed. Comparison of the effective light intensity in these experiments to a typical actinic flux at Earth's surface can be made if it is assumed that the photolysis of O_3 to generate OH, which in the troposphere occurs at 290 to 320 nm, is the key step in initiating Cl^- oxidation. Experiments in which O_3 was photolyzed in the chamber in dry N_2 gave a first-order rate constant for O_3 photolysis of $k_p = 8 \times 10^{-4}\ s^{-1}$, based on the measured rate of O_3 loss and a mechanism describing the subsequent secondary reactions in this system. In contrast, a typical calculated photolysis rate constant for O_3 to generate $O(^1D)$ at 290 to 320 nm is $7.2 \times 10^{-6}\ s^{-1}$ at a solar zenith angle of 60°. This comparison suggests that the effective light intensity in the chamber experiments is about 110 times that in the atmosphere at a solar zenith angle of 60°. Clearly, this is an approximation because the particles increase the light scattering in the chamber and light intensities within the particles themselves can be enhanced by multiple internal reflections (*36, 37*).

Applying these factors to the observed rate of Cl_2 formation in the chamber experiments (45 ppb in 2 min at an initial O_3 concentration of 14 ppm) suggests that, over 10 hours, approximately 310 ppt Cl_2 could be generated. This is similar in magnitude to the missing Cl_2 source of 280 ppt per day proposed by Spicer *et al.* at a coastal site (*21*).

Finally, if this chemistry occurs in airborne sea-salt particles, it is likely also to occur at the ocean surface. UV light penetrates the ocean surface layer (*38*). However, dissolved organics are present and they can trap significant amounts of OH before it reacts with Cl^-. (This may also be true of airborne sea-salt particles.) In addition, the aqueous-phase concentration of Cl^- in seawater is about 10% of that of saturated solutions corresponding to sea-salt particles at their deliquescence point. Thus, although the photochemical reaction of O_3 in the ocean surface layer is likely to also be a significant source of Cl_2, quantitative estimates of its contribution await additional experiments.

The subsequent photolysis of Cl_2 in the gas phase will generate atomic Cl, whose fate depends on the relative concentrations of organics and O_3. The rate constant for the reaction of Cl with most organics is $\sim 10^{-10}$ cm^3 $molecule^{-1}$ s^{-1}, about an order of magnitude faster than that for its reaction with O_3 (*39*). Even the reaction of Cl with CH_4, which is distributed globally at a concentration of 1.8 ppm, is relatively fast, with $k^{298\ K} = 1.0 \times 10^{-13}\ cm^3\ molecule^{-1}\ s^{-1}$ (*39*). If the total concentration of organics other than CH_4 is 10 ppb compared to ~40 ppb for O_3 in the remote marine boundary layer, approximately 70% of the Cl atoms will react with CH_4 and organic molecules rather than with O_3. These Cl atom reactions therefore not only contribute to the removal of organics in the marine boundary layer, but in the presence of NO_x may lead to further O_3 generation. Furthermore, these studies indicate that estimates of the net emissions of organics by the ocean to the free troposphere must also take into account their removal by Cl atoms, in addition to removal by OH and O_3, in the marine boundary layer.

Although similar bromide chemistry (*40*) should also occur to generate Br_2 or BrCl, the small amount of Br^- in the sea-salt aerosols (*41*) would have produced gaseous bromine below our detection limit. However, both Br_2 and BrCl production was observed, as expected, when the sea salt was doped with additional NaBr.

REFERENCES AND NOTES

1. T. A. Cahill, K. Wilkinson, R. Schnell, *J. Geophys. Res.* **97**, 14513 (1992).
2. B. J. Finlayson-Pitts, *Res. Chem. Intermed.* **19**, 235 (1993).
3. T. E. Graedel and W. C. Keene, *Global Biogeochem. Cycles* **9**, 47 (1995).
4. W. C. Keene, D. J. Jacob, S.-M. Fan, *Atmos. Environ.* **30**, i (1996).
5. M. O. Andreae and P. J. Crutzen, *Science* **276**, 1052 (1997).
6. B. J. Finlayson-Pitts and J. N. Pitts Jr., *ibid.*, p. 1045.
7. A. R. Ravishankara, *ibid.*, p. 1058.
8. V. Ramanathan, *ibid.* **240**, 293 (1988).
9. B. J. Finlayson-Pitts and J. N. Pitts Jr., *Atmospheric Chemistry: Fundamentals and Experimental Techniques* (Wiley, New York, 1986).
10. R. Sander and P. J. Crutzen, *J. Geophys. Res.* **101**, 9121 (1996).
11. R. Vogt, P. J. Crutzen, R. Sander, *Nature* **383**, 327 (1996).
12. H. B. Singh and J. F. Kasting, *J. Atmos. Chem.* **7**, 261 (1988).
13. W. C. Keene *et al.*, *Global Biogeochem. Cycles* **4**, 407 (1990).
14. A. Albeic-Juretic, T. Cvitas, L. Klasinc, *Ber. Bunsenges. Phys. Chem.* **96**, 493 (1992).
15. W. Behnke, V. Scheer, C. Zetzsch, in *Naturally-Produced Organohalogens*, A. Grimwall and E. W. B. deLeer, Eds. (Kluwer Academic, Dordrecht, Netherlands, 1995), pp. 375–384.
16. W. C. Keene, J. R. Maben, A. A. P. Pszenny, J. N. Galloway, *Environ. Sci. Technol.* **27**, 866 (1993).
17. A. A. P. Pszenny *et al.*, *Geophys. Res. Lett.* **20**, 699 (1993).
18. W. C. Keene, personal communication.
19. G. A. Impey, P. B. Shepson, D. R. Hastie, L. A. Barrie, *J. Geophys. Res.* **102**, 15999 (1997).
20. ______, *ibid.*, p. 16005.
21. C. W. Spicer *et al.*, in preparation.
22. The internal surfaces of the rectangular metal chamber were coated with an inert halocarbon wax (Halocarbon Products Corporation, Series 1500) to minimize wall reactions. The top of the chamber has quartz windows, above which was mounted a series of lamps for carrying out photochemical reactions. We used four low-pressure mercury lamps (UVP, XX-15S) with the major output at λ = 254 nm.
23. Two sets of White cell mirrors were mounted at opposite ends of the chamber for long-path FTIR and UV-visible spectrometry. The base path is 2 m, with a total path length of 52 m used here for both FTIR and UV spectrometry.
24. A sampling port was used to sample the gases into the API-MS for detection and measurement of halogen gases. The use of API-MS permits the unique and sensitive identification of Cl_2, Br_2, and BrCl in the negative-ion mode as a result of the generation of the parent ions Cl_2^-, Br_2^-, and $BrCl^-$, respectively, by electron transfer from O_2^- and its clusters with water and O_2 at 1 atm. We isolated the parent ion using the first quadrupole. Scans based on the use of this quadrupole provide conventional mass spectra and are called Q1 scans. Ions exiting this first quadrupole can be collisionally dissociated in a gas collision cell, and the fragment ions thus generated can be measured in the second quadrupole. Mass spectra generated by this approach are called MS-MS scans. This dual-selection process permits the unique identification of the halogens in complex mixtures.
25. D. O. DeHaan and B. J. Finlayson-Pitts, *J. Phys. Chem.*, in press.
26. H. Taube, *Trans. Faraday Soc.* **53**, 656 (1957).
27. G. R. Peyton and W. H. Glaze, *Environ. Sci. Technol.* **22**, 761 (1988).
28. M. D. Gurol and A. Akata, *AIChE J.* **42**, 3283 (1996).
29. G. G. Jayson, B. J. Parsons, A. J. Swallow, *J. Chem. Soc. Faraday Trans. 1* **69**, 1597 (1973).
30. I. Wagner, J. Karthäuser, H. Strehlow, *Ber. Bunsenges. Phys. Chem.* **90**, 861 (1986).
31. The rate constant for the dissociation at room temperature is $k_{9b} = 6.1 \times 10^9\ s^{-1}$; that for reaction 10 is $k_{10} = 2.1 \times 10^{10}$ liter $mol^{-1}\ s^{-1}$ (*29*). At a pH of 7, the lifetime of $HOCl^-$ with respect to dissociation is 0.2 ns compared to 0.5 ms for reaction 10 with H^+. Thus, reaction 10 is the rate-determining step, which is still relatively fast on the time scale of our experiments.
32. There is experimental evidence for this in these studies because peak Cl_2 concentrations decreased as

the initial O_3 concentration decreased.
33. C. D. O'Dowd and M. H. Smith, *J. Geophys. Res.* **98**, 1137 (1993).
34. S. L. Gong *et al.*, *ibid.* **102**, 3819 (1997).
35. C. D. O'Dowd, M. H. Smith, I. E. Consterdine, J. A. Lowe, *Atmos. Environ.* **31**, 73 (1997).
36. S. Madronich, *J. Geophys. Res.* **92**, 9740 (1987).
37. A. Ruggaber *et al.*, *Atmos. Environ.* **31**, 3137 (1997).
38. R. C. Smith and K. S. Baker, *Photochem. Photobiol.* **29**, 311 (1979).
39. R. Atkinson, *J. Phys. Chem. Ref. Data* **26**, 215 (1997).
40. U. von Gunten and J. Hoigné, *Environ. Sci. Technol.* **28**, 1234 (1994).
41. The molar ratio of Br$^-$ to Cl$^-$ in the aerosol is 1:660.

42. The concept, design, and construction of the aerosol apparatus was carried out in collaboration with J. C. Hemminger, F. S. Rowland, and D. W. Toohey and was supported by NSF (grant ATM-9512181) and the University of California, Irvine. We are also grateful to NSF (grant ATM-9741817), especially J. L. Moyers, and the U.S. Department of Energy (grant DE-FG-03-94ER61899) for support. We thank P. Poyner, L. Moritz, and J. Meyer for assistance with the chamber design and construction, J. N. Pitts Jr., J. Stutz, E. G. Chapman, C. M. Berkowitz, and W. C. Keene for helpful discussions, and C. W. Spicer for advice on API-MS and for providing the annual denuder.

17 September 1997; accepted 11 November 1997

Broad-Spectrum, Non-Opioid Analgesic Activity by Selective Modulation of Neuronal Nicotinic Acetylcholine Receptors

A. W. Bannon,* M. W. Decker,† M. W. Holladay, P. Curzon, D. Donnelly-Roberts, P. S. Puttfarcken, R. S. Bitner, A. Diaz, A. H. Dickenson, R. D. Porsolt, M. Williams, S. P. Arneric

Development of analgesic agents for the treatment of severe pain requires the identification of compounds that are devoid of opioid receptor liabilities. A potent (inhibition constant = 37 picomolar) neuronal nicotinic acetylcholine receptor (nAChR) ligand called ABT-594 was developed that has antinociceptive properties equal in efficacy to those of morphine across a series of diverse animal models of acute thermal, persistent chemical, and neuropathic pain states. These effects were blocked by the nAChR antagonist mecamylamine. In contrast to morphine, repeated treatment with ABT-594 did not appear to elicit opioid-like withdrawal or physical dependence. Thus, ABT-594 may be an analgesic that lacks the problems associated with opioid analgesia.

Systemic administration of opioid analgesics such as morphine remains the most effective means of alleviating severe pain across a wide range of conditions that includes acute, persistent inflammatory, and neuropathic pain states (*1*). Despite the broad-spectrum analgesic actions of the opioids, their clinical use is limited by side effects such as respiratory depression, constipation, and physical dependence as well as scheduling constraints and perceived abuse liabilities (*2*). Efforts to develop new generations of analgesics for the treatment of moderate to severe pain states based on advances in the understanding of endogenous opiate systems have resulted in only modest incremental improvements (*3*). Thus, the challenge in developing therapies for the management of severe pain has been the identification of compounds that are devoid of opioid receptor interactions and consequently of opioid-related liabilities, yet have a defined mechanism of action that is related to pain-processing mechanisms.

The antinociceptive activity of (−)−nicotine was reported as early as 1932 (*4*). However, (−)−nicotine has not been developed as an analgesic agent because of its poor spectrum of antinociceptive activity, low intrinsic activity relative to that of the opioids, and poor side-effect profile (*5*). The potent, broad-spectrum antinociceptive actions of epibatidine (*6*), an alkaloid isolated from the skin of Ecuadorian frogs, are also mediated via a neuronal nicotinic acetylcholine receptor (nAChR) mechanism (*7*). However, these antinociceptive actions are accompanied by adverse effects (for example, hypertension, neuromuscular paralysis, and seizures) at or near the doses required for antinociceptive efficacy (*8*), and these dose-limiting in vivo actions have precluded the development of epibatidine as an analgesic agent. Because these effects are mediated via interactions with distinct ganglionic, neuromuscular, and central nervous system (CNS) nAChR subtypes, the design of compounds selective for distinct nAChR subtypes is an approach to identifying analgesic agents with reduced side effects as compared to those of (±)−epibatidine. In the rodent CNS, the predominant nAChR subtypes are $\alpha 4\beta 2$ and the homooligomer $\alpha 7$ (*9*). These differ from the $\alpha_1\beta_1\delta\gamma(\varepsilon)$ and $\alpha 3$-containing nAChR subtypes found at the neuromuscular junction (*10*) and sympathetic ganglia (*11*), respectively, that mediate many of the undesired functional effects of (±)−epibatidine. A number of nAChR ligands have been reported that are selective for neuronal nAChR subtypes and may have potential in the treatment of Alzheimer's disease and Parkinson's disease (*12*).

ABT-594 [(*R*)-5-(2-azetidinylmethoxy)-2-chloropyridine] (Fig. 1) was synthesized as a potential neuronal nAChR ligand and identified as a potential analgesic agent in a mouse hot plate screen (*13*). The activity of ABT-594, (−)−nicotine, and (±)−epibatidine at $\alpha 4\beta 2$ neuronal nAChRs was determined with the use of [^{3}H]cytisine binding to rat brain membranes (Table 1) (*14*). The inhibition constant (K_i) values for the three nAChR ligands were 37 pM, 1 nM, and 42 pM, respectively. In cell membranes from *Torpedo californica* electroplax (that is, neuromuscular nAChRs), ABT-594 and (−)−nicotine were ineffective in displacing [^{125}I]α-bungarotoxin (α-bgt) binding ($K_i >$ 10 μM), whereas (±)−epibatidine had a K_i value of 2.4 nM. Thus, while ABT-594 and (±)−epibatidine have similar affinity for

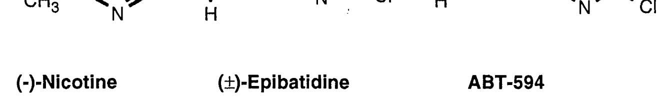

Fig. 1. The chemical structures of (−)−nicotine, (±)−epibatidine, and ABT-594 [(*R*)-5-(2-azetidinylmethoxy)-2-chloropyridine]. Like epibatidine, ABT-594 possesses a 2-chloro-5-pyridyl group and a basic nitrogen atom, but it differs structurally in several respects (*13*), including (i) the azacycle moiety encompassing the basic nitrogen atom (azetidine versus 7-azabicyclo[2.2.1]heptane); (ii) elements linking the pyridyl group to the azacycle moiety (oxymethylene versus a single bond); (iii) the smallest number of contiguous bonds intervening between the pyridine moiety and the basic nitrogen atom (four versus three); (iv) the number of freely rotatable internal bonds in the molecule (three versus one); and (v) the number of chiral centers (one versus three).

A. W. Bannon, M. W. Decker, M. W. Holladay, P. Curzon, D. Donnelly-Roberts, P. S. Puttfarcken, R. S. Bitner, M. Williams, S. P. Arneric, Neurological and Urological Diseases Research, Pharmaceutical Products Division, Abbott Laboratories, Abbott Park, IL 60064–3500. USA.
A. Diaz and A. H. Dickenson, Neuropharmacology of Pain Group, University College London, London, WC1E 6BT, UK.
R. D. Porsolt, ITEM-LABO, 94276 Le Kremlin Bicetre Cedex, France.

---

*Present address: AMGEN, Inc., Thousand Oaks, CA 91320, USA.

†To whom correspondence should be addressed. E-mail: michael.w.decker@abbott.com